International Journal of Current Research and Academic Review

ISSN: 2347-3215 Volume 3 Number 3 (March-2015) pp. 130-149

www.ijcrar.com

Structural, Spectroscopic (FT-IR, FT-Raman & UV-Vis) and theoretical studies of 4,6-Dichloro-3-formyl coumarin

R.K.Raj[1,5]* S.Gunasekaran[2], T.Gnanasambandan[2] and S.Seshadri[4]

[1]Department of Physics, SCSVMV University, Enathur, Kanchipuram-631561
[2]Research & Development, St.Peter's University, Avadi, Chennai -600 054.
[3]Department of Physics, Pallavan College of Engineering, Kanchipuram -631 502.
[4]Department of Physics, L.N.Govt.Arts College, Ponneri-601204 India.
[5]Departmet of Physics, Pachaiyappa's College for Men, Kanchipuram -631 503
Corresponding author

KEYWORDS

FTIR FT-Raman, DFT, MEP, NBO, NLO

A B S T R A C T

In this work, the vibrational spectral analysis was carried out using Raman and infrared spectroscopy in the range 4000–400 cm^{-1} and 3500–100 cm^{-1}, respectively, for the 4,6-Dichloro-3-formyl coumarin (DCFC). The experimental spectra were recorded in the solid phase. The fundamental vibrational frequencies and intensities of vibrational bands were evaluated using density functional theory (DFT) with the standard B3LYP using 6-31G (d,p) and 6-311++G(d,p) method and basis sets. Simulation of infrared and Raman spectra utilizing the results of these calculations led to excellent overall agreement with the observed spectral patterns. The complete assignments were performed on the basis of the potential energy distribution (PED) of the vibrational modes, calculated with scaled quantum mechanics (SQM) method. The stability of the molecule arising from hyper conjugative interactions and the charge delocalization has been analyzed using natural bond orbital (NBO) analysis. The directly calculated ionization potential (IP), electron affinity (EA), electronegativity (χ), electrophilicity index (ω), hardness (η) and chemical potential (μ) are all correlated with the HOMO and LUMO energies with their molecular properties. These properties show that the charge transfer occurs within the molecule. Further molecular electrostatic potential maps (MESP) of the molecule have been calculated.

Introduction

Coumarin was first synthesized in 1868. It is used in the pharmaceutical industry as a precursor reagent in the synthesis of a number of synthetic anticoagulant pharmaceuticals similar to dicoumarol, the notable ones being warfarin (brand name Coumadin) and some even more potent rodenticides that work by the same anticoagulant mechanism. Coumarins are a type of vitamin K antagonists.

Pharmaceutical coumarins were all developed from the study of sweet clover disease. coumarin is found naturally in many plants, notably in high concentration in the tonka bean.

Coumarin and its derivatives were studied by several authors. Experimental Spectroscopic (FT-IR, FT-Raman, NMR) and DFT Studies of 7-methoxy-4-bromomethylcoumarin were studied by N. Prabavathi et.al.[1]. FTIR, FT-Raman, FT-NMR and quantum chemical investigations of 3-acetylcoumarin were investigated by V.Arjunan et.al[2]. Molecular structure, vibrational spectroscopic studies and natural bond orbital analysis of 7-amino-4-trifluoromethyl coumarin was reported by M.K.Subramanian et.al.[3]. Scaled Quantum Chemical Calculations and FT-IR, FT-Raman Spectral Analysis of 4-Hydroxy-3-Nitrocoumarin was carried out by M.Sivasubramanian [4]. FT-IR, FT-Raman and UV–Vis spectra and DFT calculations of 3-cyano-4-methylcoumarin were studied earlier by N. Udaya Sri[5].

In the present work, harmonic-vibrational frequencies are calculated for 4,6-Dichloro-3-formyl coumarin (DCFC) using B3LYP with 6-31G(d,p) and 6-311++G(d,p) method. The calculated spectra of the compound are compared to that of experimentally observed FT-IR and FT-Raman spectra. The redistribution of electron density (ED) in various bonding and antibonding orbitals and E(2) energies have been calculated by natural bond orbital (NBO) analysis by DFT method to give clear evidence of stabilization originating from the hyper conjugation of various intramolecular interactions. The HOMO and LUMO analysis have been used to elucidate information regarding ionization potential (IP), electron affinity (EA), electronegativity (χ), electrophilicity index (ω), hardness (η), chemical potential (μ), and softness(S) are all correlated. These are confirming the charge transfer within the molecule and also the molecular electrostatic potential (MESP) contour map shows the various electrophilic region of the title molecule. However, molecular hyperpolarizability is also calculated by DFT method. Finally, the correlations between thermodynamic properties with various temperatures are reported.

Methods of analysis

The fine crystalline sample of DCFC is used for the spectral measurements. The FTIR spectrum was recorded by KBr pellet method on Bruker IFS 66V spectrometer equipped with a Globar source, Ge/KBr beam splitter, and a MCT detector in the range of 4000–400 cm^{-1}. The spectral resolution was 2 cm^{-1}. The FT-Raman spectrum of the compound was also recorded in the range 3500–100 cm^{-1} using the same instrument with FRA 106 Raman module equipped with Nd:YAG laser source operating at 1064 nm with 200mW power. The frequencies of all sharp bands are accurate to ±2 cm^{-1}. The ultraviolet absorption spectrum of the sample dissolved in acetone was examined in the range 200–400 nm by using Cary 5E UV–Vis recording spectrometer.

Quantum chemical calculations

The gradient corrected density functional theory (DFT) [6] with the three-parameter hybrid functional Becke3(B3) [7] for the exchange part and the Lee–Yang–Parr (LYP) correlation function [8] level of calculations have been carried out with Gaussian-03W[9] program package, invoking gradient geometry optimization [10] on a Intel Core i5/3.03 GHz processor. The combination of vibrational spectroscopy

and DFT calculations is considered to be a powerful tool for understanding the fundamental mode of vibrations and the electronic structure of the compounds. The optimised structural parameters were used in the vibrational frequency calculations. The Raman intensities were also determined with B3LYP method using 6-31G(d,p)/6-311++G(d,p) basis sets. The Raman scattering activities (Si) calculated by Gaussian 03W program were suitably converted to relative Raman intensities (Ii) using the following relationship derived from the basic theory of Raman scattering [11].

$$I_i = \frac{f(\nu_o - \nu_i)^4 S_i}{\nu_i[1-\exp(-hc\nu_i/k_bT)]}$$

where ν_o is the exciting frequency in cm^{-1}, ν_i the vibrational wave number of the i^{th} normal mode, h, c and k_b are the fundamental constants and f is a suitably chosen common normalisation factor for all the peak intensities.

Results and Discussion

Molecular geometry

The first task for the computational work is to determine the optimized geometries of the title compound. The optimized molecular structure of DCFC with the numbering scheme of the atoms is shown in Fig. 1. The optimized structural parameters such as bond lengths, bond angles are determined by B3LYP method with 6-31G(d,p) and 6-311++G(d,p) as basis sets. The geometry of the molecule is considered by possessing C1 point group symmetry. From the structural data given in Table 1, it is observed that the various benzene ring C–C bond distances and the C–H bond lengths of title compound are found to be almost same at all levels of calculations. But the bond length of C_5-Cl_{15} alone has the highest value due to the carbonyl groups compared to C-C, C-O and C-H.

Vibrational analysis

The theoretical and obtained experimental spectra (infrared and Raman spectra) are given in Figs. 2 and 3 for comparison. The recorded and computed vibrational wavenumbers along with probable vibrational description of the normal modes based on the PED are presented in Table 2. The calculated vibrational wavenumbers are higher than their experimental values for the majority of the normal modes. Two factors may be responsible for the discrepancies between the experimental and calculated results. The first is caused by the environment and the calculations were made for a free molecule in vacuum, while the experiments were performed for solid samples. The second is due to the fact that the experimental values are an anharmonic wavenumbers while the calculated values are harmonic ones. After the scaling of calculated wavenumbers, a reliable accuracy was obtained.

C–H vibration

The heteroaromatic structure shows the presence of C–H stretching vibrations in the region 3000–3100 cm^{-1} which is the characteristic region for the ready identification of this group [12]. In this region the bands are not much disturbed due to substituent. Hence, in the present study the band appeared at 3125 cm^{-1} in FT-IR spectrum and 3126 cm^{-1} in FT-Raman spectrum are assigned to C–H stretching modes of vibrations. The calculated wavenumber at 3128 cm^{-1} in B3LYP/6-31G(d.p) and 3125cm^{-1} in B3LYP/6-311++G(d,p) methods are assigned to C–H

stretching vibration. As indicated by PED, with these modes, 99% contribution comes from pure stretching vibration. The C–H in-plane and out-of-plane bending vibrations generally lie in the range 1000–1300 cm^{-1} and 950–800 cm^{-1} [13,14] respectively. Normally the bands are very weak and in the present case the band appeared at 1255 and 1120 cm^{-1} in FT-IR spectrum and 1254 and 1119 cm^{-1} at FT-Raman spectrum are assigned C–H in-plane bending vibrations. The scaled vibration predicts at 1255, 1230 and 1118cm^{-1} in B3LYP/6-31G(d,p) and 1253, 1227 and 1120 cm^{-1} in B3LYP/6-311++G(d.p) methods are assigned to C–H in-plane bending vibration show good agreement with literature [15] as well as recorded spectral data. The C–H out-of plane bending vibrations are observed at 936 and 867 cm^{-1} in FT-IR and 937 and 868 cm^{-1} in FT-Raman spectrum show good agreement with the computational methods with PED 70%.

C–Cl vibrations

The stretching vibration of C_5–Cl_{15} and C_8-Cl_{14} was observed at 1071 and 831cm^{-1} in the FT-IR spectrum and in the Raman spectrum, this is in agreement with the literature data [16,17]. In our present study the FT-Raman band observed at 141cm^{-1} was assigned to C-Cl in-plane bending vibration and the C-Cl out-of-plane bending vibration was observed at 336cm^{-1} which is in agreement with the calculated value.

Skeletal vibrations

The benzene ring possesses six stretching vibrations of which the four with highest wave numbers occurring near 1650–1400 cm^{-1} are good group vibrations [18].With heavy substituents, the bands tend to shift to somewhat lower wave numbers and greater the number of substituents on the ring, broader the absorption regions. In the title molecule, the bands observed in FT-IR and FT-Raman at 1593, 1521 and 1591, 1520 cm^{-1} have been assigned to C–C stretching are due to the substituents in benzene ring. The calculated C–C stretching vibrations using B3LYP/6-31G(d,p) shows a very good agreement with the experimental values.

C–O vibrations

The carbonyl bands are the most characteristic bands of infrared spectrum. Both the carbon and oxygen atoms of the carbonyl group move during vibration and they have nearly equal amplitudes. The carbonyl frequencies can be considered altered by intermolecular hydrogen bonding. A great deal of structural information can be derived from the exact position of the carbonyl stretching absorption peaks. Normally, carbonyl group vibrations occur in the region 1800–1700 cm^{-1}[19]. Accordingly, the FT-IR bands observed at 1807cm^{-1} and 1724 $cm^{-1}$are assigned to C–O stretching vibrations for the DCFC respectively. The C=O in-plane bending vibrations of DCFC is observed at 508cm^{-1} in IR and Raman spectrum as a strong band. The band appeared at 721 cm^{-1} in IR and 720 cm^{-1} in Raman are assigned to C=O out-of-plane bending vibrations.

Other Molecular properties

NBO analysis

NBO analysis provides the most accurate possible 'natural Lewis structure' picture of ϕ, because all orbital details are mathematically chosen to include the highest possible percentage of the electron density. A useful aspect of the NBO method is that it gives information about interactions in both filled and virtual orbital spaces that

could enhance the analysis of intra- and inter molecular interactions. The second-order Fock matrix was carried out to evaluate the donor–acceptor interactions in the NBO analysis [20]. The interactions result is a loss of occupancy from the localized NBO of the idealized Lewis structure into an empty non-Lewis orbital. For each donor (i) and acceptor (j), the stabilization energy E(2) associated with the delocalization i→j is estimated as

$$E_2 = \Delta E_{ij} = q_i \frac{F(i,j)^2}{\varepsilon_j - \epsilon_i}$$

where q_i is the donor orbital occupancy, ε_i and ε_j are diagonal elements and F(i, j) is the off diagonal NBO Fock matrix element.

Natural bond orbital analysis provides an efficient method for studying intra- and intermolecular binding and interaction among bonds, and also provides a convenient basis for investigating charge transfer or conjugative interaction in molecular systems. Some electron donor orbital, acceptor orbital and the interacting stabilization energy resulted from the second-order micro-disturbance theory are reported [21,22]. The larger the E(2) value, the more intensive is the interaction between electron donors and electron acceptors, i.e. the more donating tendency from electron donors to electron acceptors and the greater the extent of conjugation of the whole system. Delocalization of electron density between occupied Lewis-type (bond or lone pair) NBO orbitals and formally unoccupied (anti-bond or Rydberg) non-Lewis NBO orbitals correspond to a stabilizing donor–acceptor interaction. NBO analysis has been performed on the molecule at the DFT/B3LYP/6-31G(d,p) level in order to elucidate the intramolecular, re-hybridization and delocalization of electron density within the molecule. The intramolecular interaction are formed by the orbital overlap between πC–C and π*C–C bond orbital which results intramolecular charge transfer (ICT) causing stabilization of the system. These interactions are observed as increase in electron density (ED) in C–C, and O–C anti-bonding orbital that weakens the respective bonds.

The intramolecular interaction are formed by the orbital overlap between bonding π(C6-C11), π(C7-C8), π(C9-C10) and antibonding π*(C7-C8), π*(C9-C10) and π*(C6-C11) orbital which results in ICT causing stabilization of the system. The second-order perturbation theory of Fock matrix in the NBO analysis shows strong intramolecular hyperconjugative interactions and the results are presented in Table 3. The most important interactions observed are π*(C4-C5)→π*(C12-O13), π*(C7-C8)→π*(C9-C10) and π*(C6-C11)→π*(C9-C10) and the corresponding energies are 81.53, 173.92 and 278.41KJ/mol respectively. This larger energy provides the stabilization to the molecular structure.

Non-linear optical effects

Non linear optical (NLO) effects arise from the interactions of electromagnetic fields in various media to produce new fields altered in phase, frequency, amplitude or other propagation characteristics from the incident fields [23]. The first order hyperpolarizability (β_o) of this novel molecular system and related properties (β, α_o and Δα) of DCFC are calculated using B3LYP/6-31G(d,p) method based on the finite-field approach. In the presence of an applied electric field, the energy of a system is a function of the electric field. First order hyperpolarizability is a third rank tensor that can be described 3×3×3 matrices. The 27 components of the 3D matrix can be reduced

to 10 components due to the Kleimman symmetry [24]. It can be given in the lower tetrahedral format. It is obvious that the lower part of the 3×3×3 matrices is a tetrahedral. The components of β are defined as the coefficients in the Taylor series expansion of the energy in the external electric field. When the external electric field is weak and homogeneous this expansion becomes:

$$E = E^0 - \mu_\alpha F_\alpha - \frac{1}{2}\alpha_{\alpha\beta}F_\alpha F_\beta - \frac{1}{6}\beta_{\alpha\beta\gamma}F_\alpha F_\beta F_\gamma + \cdots$$

where E_0 is the energy of the unperturbed molecules, F_α is the field at the origin and μ_α, $\alpha_{\alpha\beta}$ and $\beta_{\alpha\beta\gamma}$ are the components of dipole moment, polarizability and the first order hyperpolarizabilities, respectively. The total static dipole moment μ, the mean polarizability α_0, the anisotropy of the polarizability Δα and the mean first order hyperpolarizability β, using the x, y, z components are defined as,

$$\mu = (\mu^2_x + \mu^2_y + \mu^2_z)^{\frac{1}{2}}$$

$$\alpha_0 = \frac{\alpha_{xx}+\alpha_{yy}+\alpha_{zz}}{3}$$

$$\Delta\alpha = 2^{-\frac{1}{2}}[(\alpha_{xx}-\alpha_{yy})^2+(\alpha_{yy}-\alpha_{zz})^2+(\alpha_{zz}-\alpha_{xx})^2+6\alpha^2_{xx}]^{\frac{1}{2}}$$

$$\beta_0 = (\beta^2_x + \beta^2_y + \beta^2_z)^{\frac{1}{2}}$$

and

$$\beta_x = \beta_{xxx} + \beta_{xyy} + \beta_{xzz}$$

$$\beta_y = \beta_{yyy} + \beta_{xxy} + \beta_{yzz}$$

$$\beta_z = \beta_{zzz} + \beta_{xxz} + \beta_{yyz}$$

Since the values of the polarizabilities(α) and hyperpolarizability(β) of the Gaussian 03W output are reported in atomic units(a.u), the calculated values have been converted into electrostatic units (esu) (α: 1 a.u = 0.1482×10^{-24} esu; β: 1a.u = 8.639×10^{-33}esu).

The total molecular dipole moment and first order hyperpolarizability are 5.1357 Debye and 7.9709×10^{-30} esu respectively and are depicted in Table 4. The first order hyperpolarizability is 21 times greater than that of urea (β of urea 0.3728×10^{-30} esu) obtained by B3LYP/6-31G(d,p) method. This result indicates the non linearity of the DCFC molecule.

Electrostatic potential

Molecular electrostatic potential (ESP) at a point in the space around a molecule gives an indication of the net electrostatic effect produced at that point by the total charge distribution (electron + nuclei) of the molecule and correlates with dipole moments, electronegativity, partial charges and chemical reactivity of the molecule. It provides a visual method to understand the relative polarity of the molecule. An electron density isosurface mapped with electrostatic potential surface depicts, the size, shapes, charge density and site of chemical reactivity of the molecules. Such mapped electostatic potential surface has been plotted for the title molecule using the computer software Gauss view [25]. A Projection of this surface along the molecular plane is given Fig 4. The different values of the electrostatic potential at the surface are represented by different colors: red represents the regions of the most negative electrostatic potential, blue represents the regions of the most positive electrostatic potential, and green represents the regions of zero potential. Electrostatic potential increases in the order red < orange < yellow < green < blue. In all cases, the shapes of the electrostatic potential surface is influenced by the structure and charge density distributions in the molecule with

sites close to the oxygen atom, showing region of most negative electrostatic potential. This Fig. 4 provides a visual representation of the chemically active sites and comparative reactivity of atoms. It may seen that, a region of zero potential envelopes the π system of the aromatic rings, leaving a more electrophilic region in the plane of hydrogen atoms in DCFC molecule.

Thermodynamic function analysis

The total energy of a molecule is the sum of translational, rotational, vibrational and electronic energies. i.e., E = Et + Er + Ev + Ee. The statistical thermo chemical analysis of DFC is carried out considering the molecule to be at room temperature of 298.15 K and one atmospheric pressure. The thermodynamic parameters, like rotational constant, zero point vibrational energy (ZPVE) of the molecule by DFT method (B3LYP). The variations in the zero point vibrational energy seem to be insignificant. The thermodynamic quantities such as entropy, heat capacity and enthalpy for various ranges (100–1000 K) of temperatures are determined and these results are presented in the Table 5. All the thermodynamic data provide helpful information for the further study on the title compound. From the Table 5 it can be observed that the thermodynamic parameters are increasing with temperature ranging from 100 K to 1000 K, due to the fact that the vibrational intensities of molecule with temperature.

Dipole moment reflects the molecular charge distribution and is given as a vector in three dimensions. Therefore, it can be used as descriptor to depict the charge movement across the molecule. Direction of the dipole moment vector in a molecule depends on the centers of positive and negative charge. Dipole moments are strictly determined for neutral molecule. For charged systems, its value depends on the choice of origin and molecular orientation. One of the important parameters of thermodynamics is the partition function. The partition function links thermodynamics, spectroscopy and quantum theory. The different types of partition functions are (i) translational partition function, (ii) rotational partition function, (iii) vibrational partition function and (iv) electronic partition function. Partition functions can be used to calculate heat capacities, entropies, equilibrium constants and rate constants. The variation of the thermodynamic functions such as entropy, heat capacity and enthalpy with temperature are graphically represented in Fig. 5 respectively.

Electronic absorption spectrum

The experimental UV-Visible spectrum of DCFC is shown in the Fig.6. The TD-DFT calculations predict a large number of allowed transitions in the UV–Visible spectral region[26]. The results of the TD-DFT calculations underestimate the experimentally obtained wave lengths. Calculations of molecular orbital geometry show that the visible absorption maxima of this molecule corresponds to the electron transition between frontier orbitals such as translation from HOMO to LUMO as shown in Fig.7. The λmax is a function of substitution, the stronger the donor character of the substitution, the more electrons pushed into the molecule. The theoretical calculations predict one intense electronic transition at 3.31eV with the wavelength 376nm, it shows an excellent agreement with the measured experimental data (exp = 375 nm) as shown in Table 6. The frontier orbital gap helps characterize the chemical reactivity and kinetic stability of the

molecule. A molecule with a small frontier orbital gap is more polarizable and is generally associated with a high chemical reactivity, low kinetic stability and is also termed as soft molecule.

Mulliken charges

The calculations of effective atomic charges plays an important role in the application of quantum mechanical calculations to molecular systems, because of atomic charge changes effect of dipole moment, molecular polarizability, electronic structure, acidity–basicity behavior and more a lot of properties of molecular systems[27]. Our interest is in the comparison of different methods to describe the electron distribution in DCFC as broadly as possible, and assess the sensitivity of the calculated charges to changes in: (i) the choice of the basis set (ii) the choice of the quantum mechanical method. Mullikan charges are calculated by determining the electron population of each atom as defined by basis sets. The result can, however, better be represented in graphical form as has been given in Fig. 8. From these results, it will be possible to say to the change to charge distribution by a change in basis set. Mulliken atomic charges calculated at the B3LYP/6-31G(d,p) and 6-311++G(d,p) are collected in Table.7.

Molecular orbital studies

The most widely used theory by chemists is the molecular orbital (MO) theory. It is important that Ionization Potential (IP), Electron Affinity (EA), Electrophilicity Index (ω), Chemical Potential (μ), Electronegativity (χ) and Hardness (η) be put into a MO framework. These are readily be done within the limitations of Koopman's theorem, the orbital energies of the frontier orbital is given by Fig. 7 show an orbital energy diagram for DCFC molecule. Only the HOMO and LUMO orbitals are shown. We focus on the HOMO and LUMO energies in order to determine interesting molecular/atomic properties and chemical quantities. In simple molecular orbital theory approaches, the HOMO energy (εHOMO) is related to the IP by Koopmann's theorem and the LUMO energy (εLUMO) has been used to estimate the electron affinity (EA) [28]. If $-\varepsilon HOMO \approx IP$ and $-\varepsilon LUMO \approx EA$, then the average value of the HOMO and LUMO energies is related to the electronegativity (χ) defined by Mulliken [29] with $\chi = (IP + A)/2$. In addition, the HOMO–LUMO gap is related to the hardness (η) [30–32], and also Parr et al. [33] defined global electrophilicity as a quantitative intrinsic numerical value and suggested the term electrophilicity index (ω), a new global reactivity descriptor of molecule, as $\omega = \mu^2/2$ where μ is the chemical potential takes the average value [34] i.e., $\mu = -(IP + EA)/2$. In general, the electrophiles are electron lovers or electron deficient and hence prefer to accept electrons and form bonds with nucleophiles. Thus electrophilicity is a useful structural depictor of reactivity and is frequently used in the analysis of the chemical reactivity of molecule [35]. The title molecule with low potential is a good electrophile, an extremely hard molecule has feeble electron acceptability. Consequently, a measure of molecular electrophilicity depends on both the chemical potential and the chemical hardness. Finally, the calculated HOMO–LUMO gaps are also closer to the first electronic excitation energies. The electronegativity and hardness are of course used extensively to make predictions about chemical behavior and these are used to explain aromaticity in organic compounds [36]. A hard molecule has a large HOMO–LUMO gap and a soft molecule has a small

HOMO–LUMO gap. In quantum theory, changes in the electron density of a chemical system result from the mixing of suitable excited-state wave function with the ground-state wave function. The mixing coefficient is inversely proportional to the excitation energy between the ground and excited state. A small HOMO–LUMO gap automatically means small excitation energies to the manifold of excited states. Therefore, soft molecule, with a small gap, will have their electron density changed more easily than a hard molecule. In terms of chemical reactivity, we can conclude that soft molecule will be more reactive than hard molecule. On the basis of a fully optimized ground state structure, the DFT/B3LYP/6-311++G(d,p) calculation predicts one intense electronic transition from the ground to the first excited state and is mainly described by one electron excitation from the highest occupied molecular orbital (HOMO) to the lowest unoccupied molecular orbital (LUMO). The HOMO is located over Cl atom and CO group, and the HOMO→LUMO transition implies an electron density transfer to the aldehydic group. Moreover, these orbitals significantly overlap in their position for DCFC. The atomic orbital compositions of the frontier molecular orbital are sketched in Fig. 7. The HOMO–LUMO energy gap of DCFC were calculated at the B3LYP/6-31G(d,p) level, which reveals that the energy gap reflects the chemical activity of the molecule. The LUMO as an electron acceptor represents the ability to obtain an electron and HOMO represents the ability to donate an electron. The energy gap between the HOMO and the LUMO molecular orbitals is a critical parameter in determining molecular electrical transport properties because it is a measure of electron conductivity. The energy values of HOMO are computed –0.31287, and –0.27050 eV and LUMO are –0.22004, –0.12819 eV and the energy gap values are 0.09283 and 0.14231 eV of DCFC, respectively. Lower value in the HOMO and LUMO energy gap explains the eventual charge transfer interactions taking place within the molecule. The calculated chemical hardness (η), chemical potential (μ), electrophilicity values (ω), ionization potential (IP), electron affinity (EA), electronegativity (χ) are presented in Table 8.

Conclusion

Attempts have been made in the present work for the proper vibrational bands assignments for the compound DCFC from FT-IR and FT Raman spectra. The equilibrium geometries and harmonic wavenumbers of DCFC were determined and analyzed by B3LYP/6-31G(d,p) and B3LYP/6-311++G(d,p) levels of theory. The predicted harmonic frequencies were compared with the experimental data. NBO analysis has been shown that, the stabilization energies have been calculated from second order perturbation theory. The energies of one electron excitation from the highest occupied molecular orbital (HOMO) to the lowest unoccupied molecular orbital (LUMO) values are calculated. Finally, the electrostostatic potential surfaces (ESP) together with complete analysis of the vibrational spectra of both IR , Raman and electronic spectra help to identify the chemically active sites of the molecule. The statistical thermodynamic parameters of DCFC for range of temperature 100–1000 K were calculated theoretically. The theoretically computed wavenumbers in both the methods were found to be good agreement with experimental FT-IR and FT-Raman results.

Table.1 Optimized geometrical parameters of DCFC

Bond length	B3LYP		Bond angle	B3LYP	
	6-31G(d,p)	6-311++G(d,p)		6-31G(d,p)	6-311++G(d,p)
O1-C2	1.404	1.405	C2-O1-C11	123.4	123.5
O1-C11	1.353	1.351	O1-C2-O3	116.8	116.8
C2-O3	1.198	1.191	O1-C2-C4	116.1	116.0
C2-C4	1.479	1.478	O3-C2-C4	126.9	127.1
C4-C5	1.368	1.366	C2-C4-C5	119.5	119.4
C4-C12	1.494	1.494	C2-C4-C12	118.2	118.5
C5-C6	1.445	1.443	C5-C4-C12	122.2	121.9
C5-Cl15	1.754	1.752	C4-C5-C6	122.4	122.5
C6-C7	1.409	1.408	C4-C5-Cl15	121.0	120.9
C6-C11	1.409	1.406	C6-C5-Cl15	116.5	116.4
C7-C8	1.383	1.380	C5-C6-C7	124.8	124.8
C7-H16	1.081	1.080	C5-C6-C11	116.3	116.4
C8-C9	1.403	1.400	C7-C6-C11	118.7	118.7
C8-Cl14	1.753	1.753	C6-C7-C8	119.7	119.7
C9-C10	1.386	1.383	C6-C7-H16	119.9	119.9
C9-H17	1.083	1.082	C8-C7-H16	120.2	120.2
C10-C11	1.398	1.395	C7-C8-C9	121.1	121.1
C10-H18	1.083	1.082	C7-C8-Cl14	119.6	119.6
C12-O13	1.211	1.205	C9-C8-Cl14	119.2	119.2
C12-H19	1.104	1.102	C8-C9-C10	119.7	119.7
			C8-C9-H17	119.8	119.8
			C10-O9-H17	120.4	120.3
			C9-C10-C11	119.6	119.6
			C9-C10-H18	121.5	121.4
			C11-C10-H18	118.1	118.8
			O1-C11-C6	122.0	121.9
			O1-C11-C10	116.9	117.1
			C6-C11-C10	120.9	120.9
			C4-C12-O13	125.1	125.3
			C4-C12-H19	113.8	113.8
			O13-C12-H19	121.0	120.7

Table.2 Vibrational Assignments of DCFC

Mode No.	Experimental		Caculated B3LYP		Vibrational Assignments + PED(%)
	FT-IR υcm^{-1}	FT-R υcm^{-1}	6-31G(d,p) Scaled υcm^{-1}	6-311++G(d,p) Scaled υcm^{-1}	
1	3125	3126	3128	3125	υCH(99)
2	3115	3117	3114	3109	υCH(99)
3	3102	3102	3102	3097	υCH(98)

4	2879	2880	2878	2879	υCH(99)
5	1807	1807	1807	1791	υOC(89)
6	1724	1722	1724	1706	υOC(95)
7	1593	1591	1593	1586	υCC(51)
8	1558	1557	1564	1558	υCC(43)
9	1521	1520	1521	1512	υCC(56)
10	1447	1447	1453	1447	υCC(23)+βHCC(37)
11	1405	1404	1405	1401	βHOC(62)
12	1376	1375	1381	1376	υCC(12)+βHOC(31)+βCCC(11)
13	1318	1319	1327	1318	υCC(67)
14	1265	1265	1272	1265	υCC(16)+βCCC(18)+βOCC(11)
15	1255	1254	1255	1253	υOC(17)+βHCC(65)
16	1227	1227	1230	1227	υOC(21)+βCCC(14)+βHCC(16)
17	1175	1175	1175	1167	υCC(60)
18	1120	1119	1118	1120	υCC(12)+βHCC(57)
19	1071	1071	1073	1071	υCC(37)+υClC(13)+βHCC(29)
20	974	972	972	974	τHCCC(62)+τOCCC(26)
21	948	949	949	948	υOC(37)+βOCO(10)
22	936	937	936	944	γHCCC(80)
23	930	928	927	930	υOC(12)+βCCC(28)
24	879	878	880	879	υOC(13)
25	867	868	867	872	γHCCC(73)+τCCCC(10)
26	831	831	831	832	υCC(10)+υClC(24)
27	815	814	812	815	τHCCC(78)+γOCCC(12)
28	721	720	717	721	τCCCC(12)+γOCOC(22)+γCCCC(21)
29	712	712	711	712	βCCC(15)+βOCC(33)
30	699	700	699	710	τOCOC(54)+τOCCC(11)
31	671	671	671	672	βCCC(16)+υCC(12)+υClC(12)
32	623	621	620	623	βCCC(39)
33	608	606	603	608	τCCCC(13)+γClCCC(37)+γCCCC(13)
34	535	534	535	535	υOC(25)+νClC(21)+βCOC(11)+βOCO(11)
35	514	513	513	514	τCCCC(13)+γClCCC(29)+γOCCC(23)
36	508	508	508	510	βCOC(12)+βOCO(20)+βOCC(33)+βCCC(11)
37	429	428	426	429	τCCCC(55)+γCCCC(10)
38	399	397	394	396	υClC(10)+βCOC(20)+βClCC(17)
39	-	380	380	382	υClC(42)+βCCC(10)
40	-	343	343	343	υCC(35)+βClCC(11)
41	-	336	337	333	τCCCC(13)+γClCCC(34)+γOCCC(26)
42	-	301	300	299	υClC(12)+βCCC(11)+βOCC(17)
43	-	274	273	274	βClCC(71)
44	-	268	272	268	βOCC(13)+βCCC(16)+τHCCC(10)+γCCCC(53)

45	-	217	217	215	βCCC(58)
46	-	149	150	145	τCCCC(21)+γClCCC(30)+γCCCC(11)
47	-	141	142	142	βCCC(35)+βClCC(50)
48	-	129	129	126	τCOCC(25)+γClCCC(18)+γOCCC(10)γCCCC(26)
49	-	-	78	62	τCCCC(49)
50	-	-	47	43	τCCCC(40)+τCOCC(40)
51	-	-	25	23	τOCCC(56)

υ- stretching; β: in-plane-bending; γ: out-of-plane bending; τ- torsion

Table.3 Second order perturbation theory analysis of Fock matrix in NBO analysis

Donor(i)	Acceptor(j)	E(2)[a] (kJ/mol)	E(j)–E(i)[b] (a.u.)	F(i, j)[c] (a.u.)
π(C6-C11)	π*(C7-C8)	21.91	0.27	0.069
π(C7-C8)	π*(C9-C10)	20.34	0.28	0.068
π(C9-C10)	π*(C6-C11)	22.14	0.26	0.070
LP(2) O1	π*(C2-O3)	26.18	0.34	0.084
LP(2) O1	π*(C6-C11)	34.01	0.33	0.100
LP(2) O3	σ*(O1-C2)	44.26	0.46	0.128
LP(2) O13	σ*(C4-C12)	24.03	0.65	0.113
π*(C4-C5)	π*(C12-O13)	81.53	0.01	0.066
π*(C6-C11)	π*(C9-C10)	278.41	0.01	0.079
π*(C7-C8)	π*(C9-C10)	173.92	0.01	0.075

Table.4 NLO properties of DCFC

Parameters	B3LYP		Parameters	B3LYP	
	6-31G(d,p)	6-311++G(d,p)		6-31G(d,p)	6-311++G(d,p)
μx	-4.9760	5.4366	βxxx	687.870	-777.111
μy	1.2497	1.6024	βxxy	419.174	460.789
μz	0.2306	0.3494	βxyy	166.284	-164.115
μ	5.1357	5.6786	βyyy	-60.0327	-67.1350
αxx	232.607	251.903	βxxz	-0.02959	-0.118972
αxy	-3.783	4.594	βxyz	0.006010	-0.0184416
αyy	142.734	157.856	βyyz	0.029076	-0.0598210
αxz	0.010	-0.116	βxzz	-6.04662	57.0335
αyz	-0.001	-0.019	βyzz	2.23817	5.38010
αzz	47.763	73.340	βzzz	37.9586	-0.016639
αtot(esu)	2.090×10^{-23}	2.386×10^{-23}	βtot(e.s.u)	7.970×10^{-30}	8.380×10^{-30}
Δα	433.53203	462.927243			

Table.5 Thermodynamic functions of DCFC

Temperature	Entropy		Enthalpy		Heat Capacity	
	B3LYP		B3LYP		B3LYP	
	6-31G(d,p)	6-311++G(d,p)	6-31G(d,p)	6-311++G(d,p)	6-31G(d,p)	6-311++G(d,p)
100.00	331.57	317.63	93.10	85.54	6.24	5.66
200.00	414.67	395.22	152.73	144.47	18.57	17.20
298.15	485.73	462.96	205.61	197.31	36.22	34.02
300.00	487.01	464.19	206.54	198.24	36.60	34.39
400.00	552.88	527.69	252.07	243.91	59.60	56.57
500.00	613.20	586.20	288.48	280.43	86.71	82.86
600.00	668.42	639.96	316.94	308.93	117.03	112.39
700.00	719.02	689.32	339.21	331.22	149.89	144.44
800.00	765.51	734.75	356.85	348.85	184.72	174.48
900.00	808.39	776.68	371.02	363.00	221.17	214.10
1000.00	848.10	815.55	382.56	374.51	258.84	250.99

Table.6 UV-Vis excitation energy(□E) of DCFC

States	TD-B3LYP/6-31G(d,p)				Expt. λ(nm)
	Gas phase		Acetone		
	λcal (nm)	E(eV)	λcal(nm)	E(eV)	
S1	413.24	3.0003	412.74	3.0039	410
S2	376.61	3.3185	364.34	3.4029	375
S3	293.76	4.2205	293.28	4.2275	295

Table.7 Mulliken atomic charges of DCFC

Atoms	B3LYP		Atoms	B3LYP	
	6-31G(d,p)	6-311++G(d,p)		6-31G(d,p)	6-311++G(d,p)
O1	-0.512752	-0.104727	C11	0.310677	-0.880845
C2	0.582863	0.261476	C12	0.262822	-0.246399
O3	0.402441	-0.206484	O13	-0.370751	-0.205514
C4	-0.022893	0.622917	Cl14	0.006239	0.517804
C5	-0.155788	-0.112342	Cl15	0.061642	0.726331
C6	0.127330	0.689411	H16	0.143209	0.219241
C7	-0.112186	-1.211766	H17	0.131473	0.205751
C8	-0.107622	0.412232	H18	0.133327	0.217049
C9	-0.064811	-0.414638	H19	0.093609	0.135097
C10	-0.103946	-0.624588			

Table.8 Molecular properties of DCFC

Molecular properties	B3LYP		Molecular properties	B3LYP	
	6-31G(d,p)	6-311++G(d,p)		6-31G(d,p)	6-311++G(d,p)
εHOMO(eV)	-0.31287	-0.27050	Chemical hardness(η)	0.046415	0.071155
εLUMO(eV)	-0.22004	-0.12819	Chemical potential(μ)	-0.266455	-0.199345
ε(H-L) (eV)	-0.09283	-0.14231	Electronegativity(χ)	0.266455	0.199345
Ionization potential(I)	0.31287	0.27050	Electrophilicity index(ω)	0.0354991	0.019868
Electron affinity(A)	0.22004	0.12819	Softness(S)	21.54475	14.053826

Fig.1 Optimized structure of DCFC

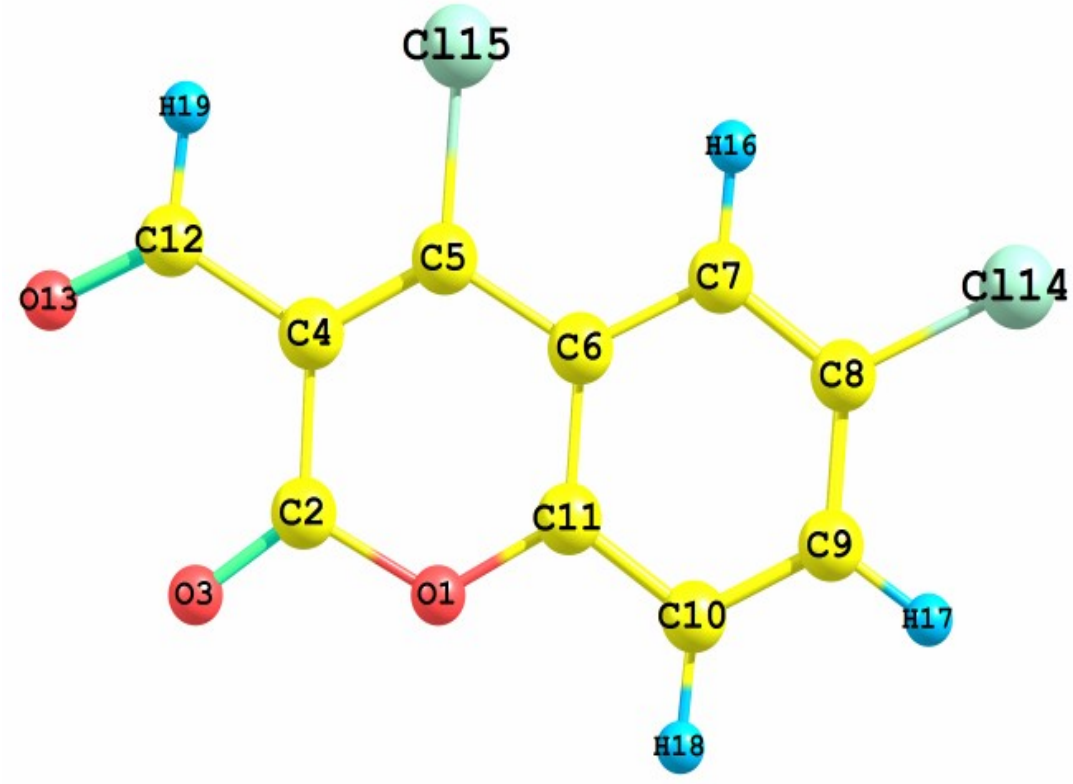

Fig.2 FT-IR spectra of DCFC

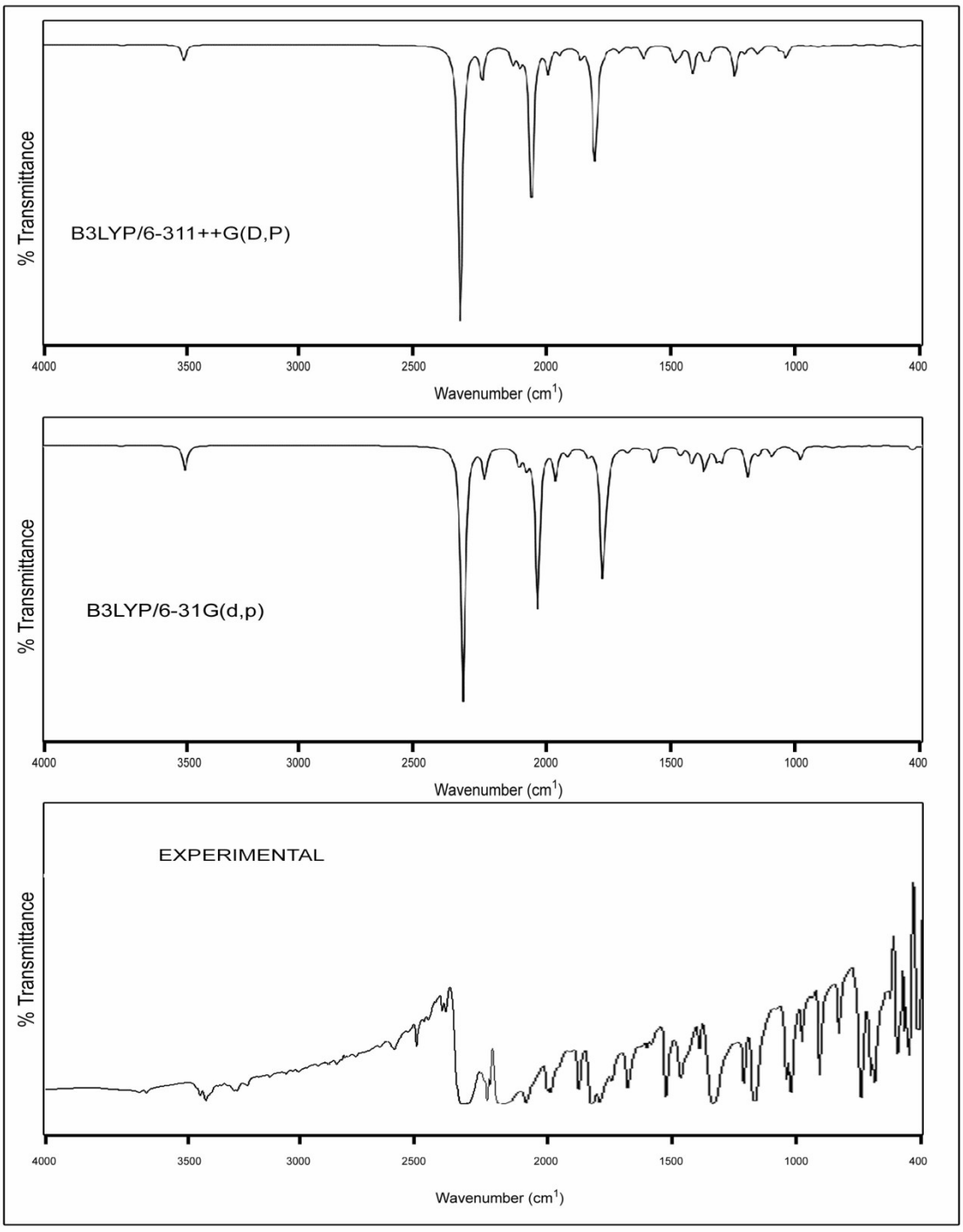

Fig.3 FT-R spectra of DCFC

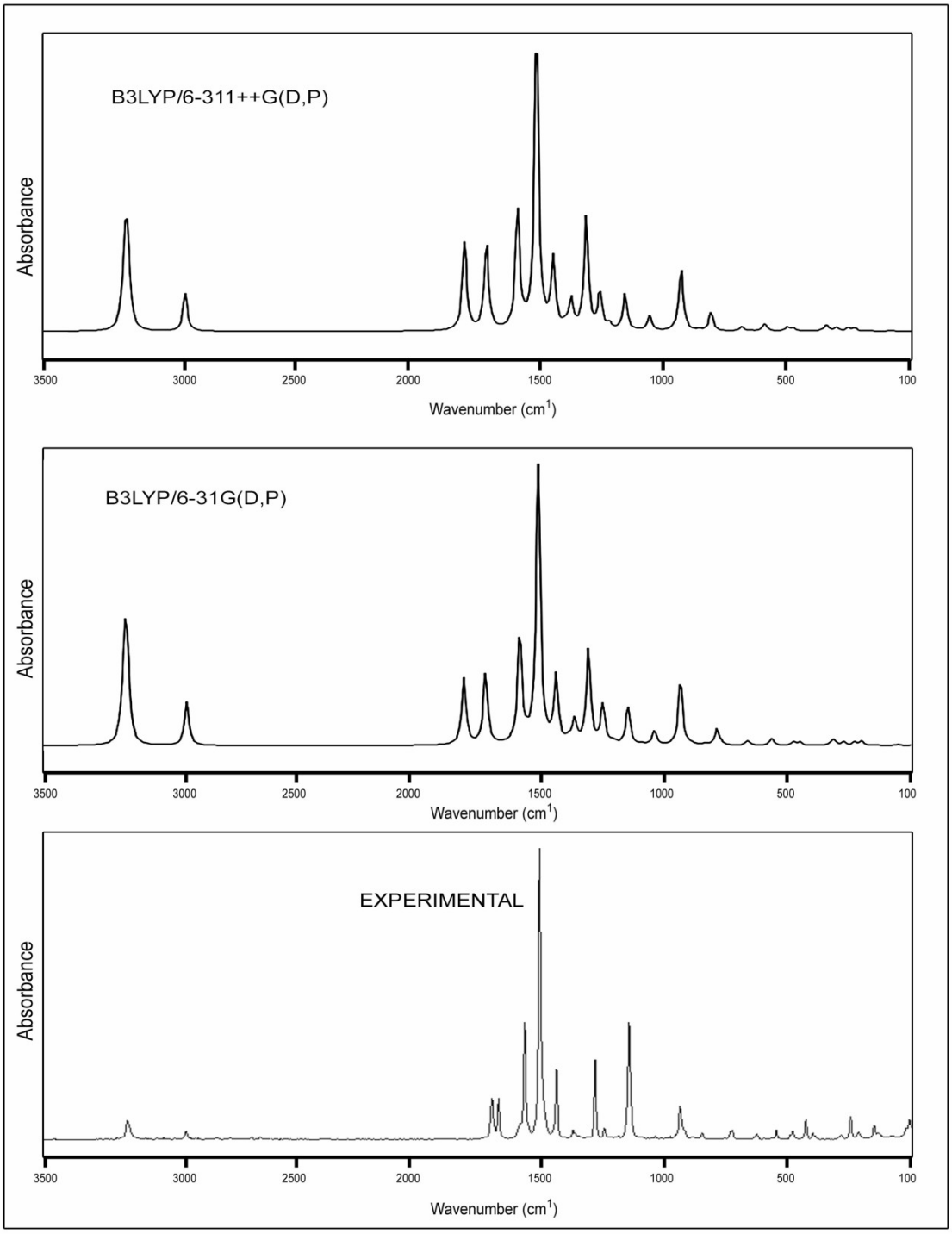

Fig.4 Molecular electrostatic potential of DCFC

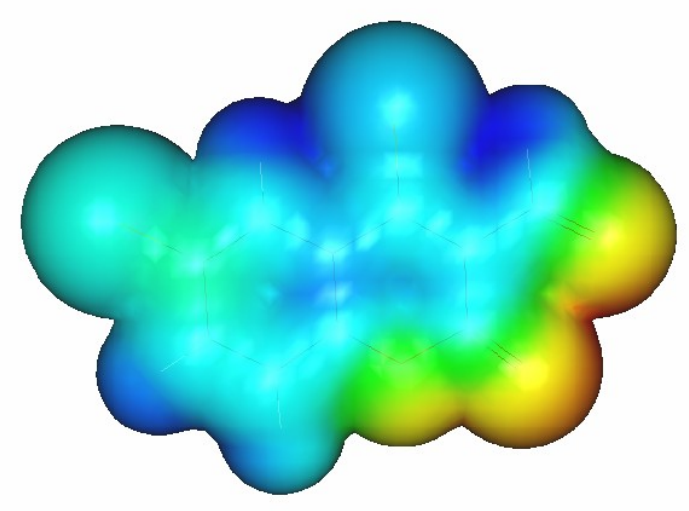

Fig.5 Thermodynamic properties of DCFC

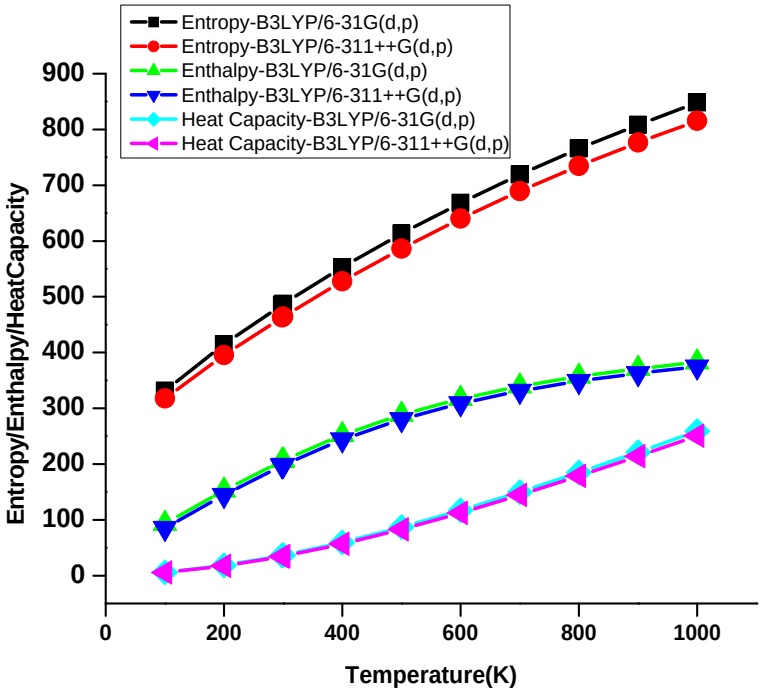

Fig.6 Experimental UV-Visible spectrum of DCFC

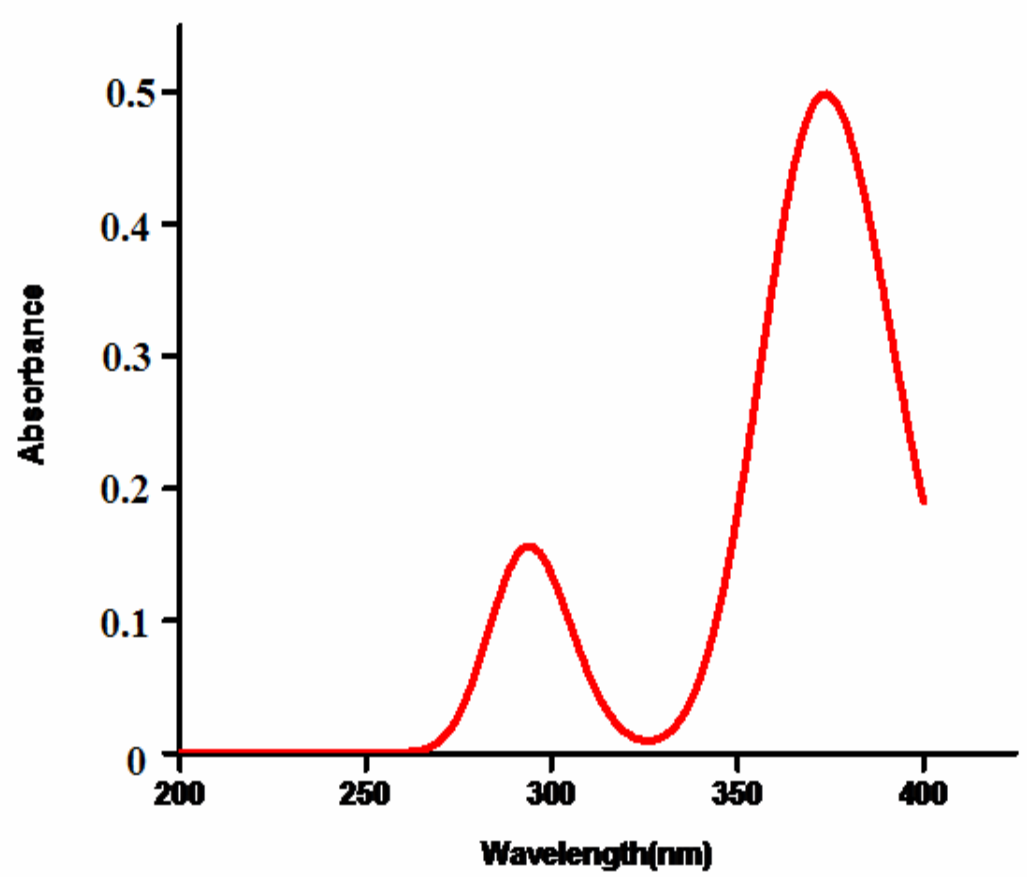

Fig.7 Frontier molecular orbital's of DCFC

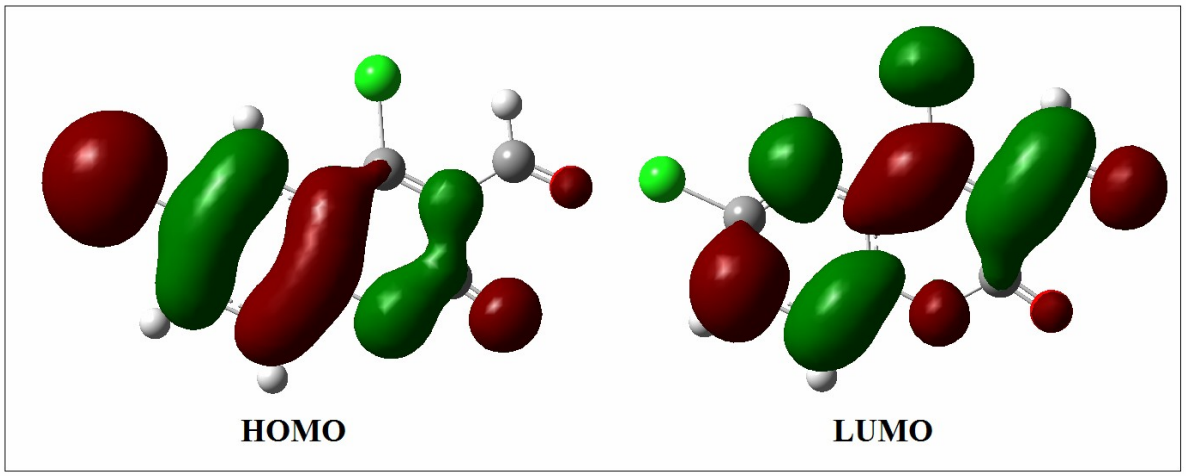

Fig.8 Mulliken charges of DCFC

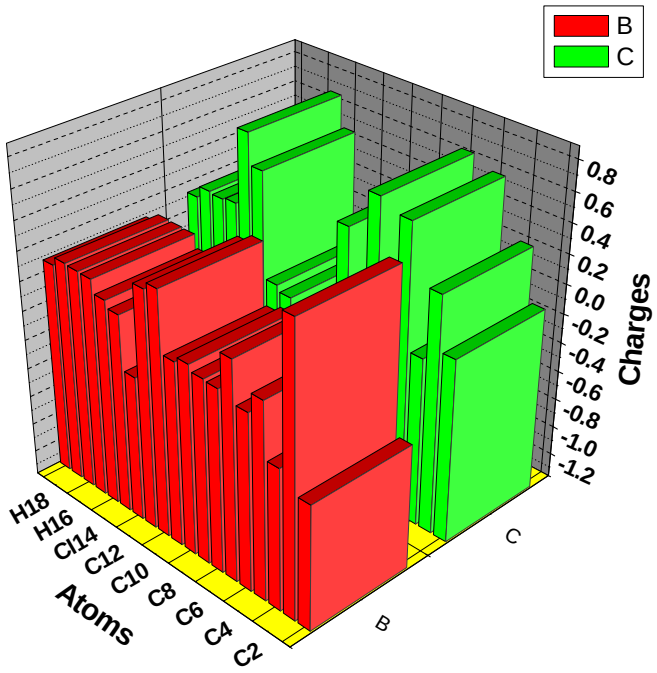

References

1.N. Prabavathi N. Senthil Nayaki J. Environ. Nanotechnol. Volume 3, No.2 pp. 108-121

2.V.Arjunan, S.Sakiladevi, M.K.Marchewka,S.Mohan , Spectrochim. Acta 109(2013) 79-89

3.M.K.Subramanian, P.M.Anbarasan,S. Manimegalai PRAMANA-Journal of physics, 74, 5(2010) 845-860

4.M. Sivasubramanian, Int.J Engg. Research & Technology, 1(7), 2012, 278-288

5.N. Udaya Sri, K. Chaitanya, M.V.S. Prasad, V. Veeraiah, A. Veeraiah , Spectrochim. Acta 97(2012) 728-736

6.P. Hohenberg, W. Kohn, Phys. Rev. 136 (1964) B864.

7.A.D. Becke, J. Chem. Phys. 98 (1993) 5648.

8.C. Lee, W. Yang, R.G. Parr, Phys. Rev. B 37 (1988) 785.

9.Gaussian Inc., Gaussian 03 Program, Gaussian Inc., Wallingford, CT, 2004.

10.H.B. Schlegel, J. Comput. Chem. 3 (1982) 214.

11.T.Gnanasambandan, S.Gunasekaran, S.Seshadri, Spectrochim. Acta A 112 (2013) 52–61.

12.Varsanyi, Assignment for Vibrational Spectra of Seven Hundred Benzene Derivatives, vol. 1–2, Academic Kiaclo, Budapest, 1973.

13.T.Gnanasambandan, S.Gunasekaran, S.Seshadri, Spectrochim. Acta A 122 (2014) 542–552.

14.D. Becke, J. Chem. Phys. 98 (1993) 5648–5652.

15.V. Krishnakumar, R. Ramasamy, Spectrochim. Acta Part A 69 (2008) 8–17.

16.P. Alcolea, M. Rastogi, V.K. Mittal, Int. J. Quantum Chem. 94 (2003) 189–204.
17.T.Gnanasambandan, S.Gunasekaran, S.Seshadri, Journal of Molecular Structure 1061 (2014) 124–133.
18.B.S. Yadav, I. Ali, P. Kumar, P. Yadav, Indian J. Pure Appl. Phys. 45 (2007) 979–983.
19.G. Socrates, Infrared and Raman Characteristic Group Frequencies – Tables and Charts, third ed., Wiley, Chichester, 2001.
20.M. Szafran, A. Komasa, E.B. Adamska, J. Mol. Struct-Theochem 827 (2007) 101–107.
21.C. James, A. Amal Raj, R. Reghunathan, I.H. Joe, V.S. Jayakumar, J. Raman Spectrosc. 37 (2006) 1381–1392.
22.J.N. Liu, Z.R. Chen, S.F. Yuan, J. Zhejiang Univ. Sci. B6 (2005) 584–591.
23.Y.X. Sun, Q.L. Hao, W.X. Wei, Z.X. Yu, L.D. Lu, X. Wang, Y.S. Wang, J. Mol. Struct. (Theochem) 904 (2009) 74.
24.D.A. Kleinman, Phys. Rev. 126 (1962) 1977.
25.M.J. Frisch, A.B. Nielsm, A.J. Holder, Gaussview User Manual, Gaussian Pitsburgh, 2008.
26.L. Lang, Absorption Spectra in the Ultraviolet and Visible Region, vol. 2, 1961, p. 159.
27.R.S. Mulliken, J. Chem. Phys. 23 (1995) 1833–1840.
28.P. Politzer, F. Abu-Awwad, Theor. Chem. Acta 99 (1998) 83.
29.R.S. Mulliken, J. Chem. Phys. 2 (1934) 782.
30.R.G. Parr, R.G. Pearson, J. Am. Chem. Soc. 105 (1983) 7512.
31.R.G. Parr, W. Yang, Density Functional Theory for Atoms and Molecules, Oxford University Press, New York, 1982.
32.R.G. Pearson, Chemical hardness, John Wiley-VCH, Weinheim, 1997.
33.R.G. Parr, L. von Szentpaly, S. Liu, J. Am. Chem. Soc. 121 (1999) 1922–1924.
34.J. Padmanabhan, R. Parthasarathi, V. Subramanian, P.K. Chattaraj, J. Phys. Chem. A 111 (2007) 1358–1361.
35.P.K. Chattaraj, B. Maiti, U. Sarkar, J. Phys. Chem. A 107 (2003) 4973–4975.
36.F. De Proft, P. Geerlings, Chem. Rev. 101 (2001) 1451.